RAD51 Enhances Zygotic Interhomolog Repair

Jonathan J. Wilde[1], Tomomi Aida[1], Martin Wienisch[1], Qiangge Zhang[1], Peimin Qi[1], and Guoping Feng[1,2*]

Affiliations:

[1]McGovern Institute for Brain Research, Department of Brain and Cognitive Sciences, Massachusetts Institute of Technology (MIT), Cambridge, Massachusetts 02139, USA

[2]Stanley Center for Psychiatric Research, Broad Institute of MIT and Harvard, Cambridge, Massachusetts 02142, USA

***Correspondence to G.F.:** fengg@mit.edu

Recent advances in CRISPR/Cas-based genome editing, including three-component CRISPR[1], the use of long single-strand donors[2], enhanced microhomology-mediated end-joining (MMEJ)[3], and pharmacological approaches[4-7] have greatly improved knock-in (KI) efficiency. In our search for factors to further improve KI efficiency for broad therapeutic use and efficient generation of primate disease models, we found that the strand exchange protein RAD51 can significantly increase homozygous KI efficiency using CRISPR/Cas9 in mouse embryos through an interhomolog repair (IHR) mechanism. Using a variety of approaches, we demonstrate robust enhancement of zygotic IHR by RAD51 and show that this can be leveraged both for generating homozygous KI animals from wildtype zygotes with exogenous donors and for converting heterozygous alleles into homozygous alleles without exogenous templates. Thus, our study provides both conclusive evidence supporting the existence of zygotic IHR mechanisms and a new method to significantly improve IHR efficiency for potential therapeutic use.

We previously described a three-component CRISPR approach, which employs Cas9 protein and chemically synthesized crRNA and tracrRNA for efficient KI of transgenes[1,2,8]. Additional published work in rabbit embryos has shown significant enhancement of KI efficiency using RS-1, a chemical agonist of the homology-directed repair (HDR) pathway member RAD51[6]. We began our study by attempting to use a combination of these techniques for high-efficiency knock-in of an autism-associated point mutation in *Chd2* (c.5051G>A; R1685H in human, R1684H in mouse; hereon referred to as *Chd2*^{R1684H}*;* **Fig. 1a**) using a single-stranded oligonucleotide donor (ssODN). Previous studies have shown that KI efficiency is affected by the proximity of the Cas9 cut site and the insertion site[9], so we chose a guide positioned where the cut site is directly adjacent to the desired G>A point mutation. Genotyping

of mouse embryos after pronuclear injection and *in vitro* culture with or without RS-1 (7.5μM) showed a high KI efficiency at the targeted *Chd2* locus, but revealed that RS-1 did not affect KI efficiency (**Extended Data Fig. 1**). Although the known mechanisms of RAD51 function suggest it may not promote knock-in with ssODNs, our previous success using exogenous protein to promote high-efficiency KI[1,2,3,8] and the fact that RS-1 can be highly dosage-sensitive[6] led us to hypothesize that the use of exogenous RAD51 protein in combination with three-component CRISPR could potentially increase KI efficiency. We first performed both pronuclear (PNI) and cytoplasmic (CPI) injections of crRNA, tracrRNA, Cas9, ssODN (30 ng/μL for PNI and 100 ng/μL for CPI), and RAD51 protein in mouse zygotes and genotyped the resulting F_0 pups (example chromatograms in **Fig. 1b**). In 18 pups, we observed an overall KI efficiency of 61.1% (**Fig. 1c**) and, surprisingly, a homozygous KI efficiency of 55.5% (**Fig. 1d**). We did not observe significant differences in efficiency between CPI and PNI (**Extended Data Fig. 2**), so we focused on PNI for the remainder of this study. Although we performed all genotyping of these animals using primers sitting outside of the homology arms, we could not rule out the possibility that the homozygous animals were actually compound heterozygotes with large deletions encompassing the cut site on one allele[10]. We therefore bred 6 of the F_0 homozygous KI mice with wildtype C57BL/6N animals and genotyped the resulting F_1 progeny. Sanger sequencing showed that all 36 F_1 pups were heterozygous mutants, confirming the homozygosity of F_0 animals (**Fig. 1e**).

Since we did not initially generate *Chd2*^{R1684H} mice with injections lacking RAD51, we performed additional injections to directly assess the ability of RAD51 to increase KI efficiency. Zygotic injections were performed with and without RAD51, embryos were cultured for two days, and nested PCR was performed for genotyping. Sanger sequencing revealed that RAD51

only slightly increased overall KI efficiency (**Fig. 2a**, left, $p<0.05$, one-tailed chi-square test), but drastically increased homozygous KI efficiency (**Fig. 2a, right**, $p<0.0001$, one-tailed chi-square test). It is widely accepted that CRISPR/Cas9-mediated editing efficiency can be highly locus- and guide-dependent, so we investigated the effects of RAD51 at a second genomic locus to confirm its efficacy. Using the same injection strategy employed for *Chd2*, we attempted to knock in an albinism-associated human mutation (c.265T>A; C89S; hereon referred to as Tyr^{C89S}; schematic in **Fig. 2b**) in the *Tyr* gene[11], which encodes for tyrosinase, the rate-limiting enzyme in melanin production. Albinism is a recessive disorder and, as such, only homozygous mutation of *Tyr* results in mice completely lacking pigment (**Fig. 2c, d**). However, indel-induced disruption of *Tyr* can also result in albinism, so all F_0 animals were genotyped to assess the effects of RAD51. Injections without RAD51 showed a high overall KI efficiency, but this efficiency was not significantly affected by the addition of RAD51 (**Fig. 2e, left**). However, our genotyping results again indicated that RAD51 can significantly increase homozygous KI efficiency, with 44.4% of pups exhibiting an albino phenotype resulting from homozygous KI of the Tyr^{C89S} allele with RAD51, as compared to only 12% without (**Fig. 2e, right**).

Strikingly, RAD51 co-injection more than doubled the observed homozygosity at both the *Chd2* and *Tyr* loci (**Fig. 2a, e**). Previous attempts to increase HDR through pharmacological or genetic mechanisms have not shown such high homozygosity rates[7,9,12], leading us to question the mechanism by which RAD51 can promote such an outcome. Our evidence that RAD51 does not strongly affect overall efficiency of ssODN-mediated knock-in (**Fig. 2a,d**) suggested that its effects on homozygosity do not come from directly increasing independent KI events on both alleles. Additionally, due to the random nature of insertion-deletions (indels) produced by non-homologous end joining (NHEJ), we found it surprising that we observed multiple embryos from

both *Chd2*^{R1684H} and *Tyr*^{C89S} injections whose genotyping results suggested the presence of the same indel on both alleles (**Extended Data Fig. 3**). Genotyping of F_1 pups derived from a female with such a homozygous indel revealed that all pups were heterozygous for the same indel, indicating that the phenomenon was not due to an indel on one allele and a large deletion encompassing the cut site on the other (**Extended Data Fig. 3**). Although we could not rule out that these deletions were generated by MMEJ, which can result in stereotyped indels based on local homology[3,13], the variety of observed indels suggested that the homozygosity resulted from recombination between homologs that transferred the KI or indel allele from one chromosome to the other.

More than 20 years ago, experiments in mouse ES cells found evidence of recombination events between homologous chromosomes[14,15]. While these interhomolog repair (IHR) events are now well-understood in meiotic cells, their occurrence in zygotes and somatic cells is poorly described. However, recently published data from experiments attempting to correct a 4bp GAGT deletion in *MYBPC3* in human embryos support a potential zygotic IHR mechanism whereby one allele can serve as the repair template for the other after induction of a targeted double-strand break (DSB) by Cas9[16]. Based on these data, we hypothesized that RAD51 promotes homozygous KI through a similar mechanism. To test this, we first performed PNI using an injection mixture containing an equimolar ratio of two separate ssODNs containing different point mutations at the same loci, allowing us to identify independent knock-in events via the observation of compound heterozygosity (**Fig. 3a**). In line with our previous observations (**Fig. 2a**), we found that co-injection of RAD51 significantly increased homozygous KI efficiency **(Fig. 3b)**. Strikingly, compound heterozygosity was observed in 5/12 control embryos with a KI event on both alleles, but was not observed in any RAD51-injected embryos (**Fig. 3b**),

supporting our hypothesis that RAD51 increases homozygosity through an enhanced IHR mechanism. Importantly, we did not observe significant differences in overall KI rates between the two ssODNs (**Extended Data Fig. 4**), ruling out the possibility that our observations were due to a bias toward one donor over the other.

In order to more directly test the IHR mechanism, we attempted to generate homozygous *Chd2*^{R1684H} embryos without the use of an exogenous donor through homozygous conversion. Using *in vitro* fertilization (IVF) with wildtype C57Bl/6N eggs and sperm from homozygous *Chd2*^{R1684H} male mice, we generated heterozygous zygotes and specifically targeted Cas9 to the maternal *Chd2* locus. As illustrated in **Figure 3c**, PNI was performed on zygotes at ~8 hours post fertilization (hpf) using a mixture of crRNA, tracrRNA, and Cas9 with or without RAD51. Because the *Chd2*^{R1684H} allele contains mutations in both the guide sequence and its associated PAM, Cas9 is only capable of cutting the wildtype maternal allele (**Extended Data Fig. 5**). Therefore, by omitting the donor template from the injection mixture we were able to directly test both the rate of baseline CRISPR/Cas9-mediated IHR in the zygote and the ability of RAD51 to enhance such a mechanism. In support of data published by Ma *et al*., we observed IHR events in 26% of control-injected embryos (**Fig. 3d,e**). Strikingly, co-injection of RAD51 was capable of increasing this rate to 74% (**Fig. 3e**). To directly rule out the possibility of false positives resulting from monoallelic deletions on the maternal allele, we developed and performed a genomic qPCR assay to analyze copy number at the targeted locus (**see Methods**). First, using genomic DNA from wildtype mice and *Shank3B*$^{+/-}$ mice harboring a heterozygous deletion of exon 13 of *Shank3*[17], we confirmed that our method was capable of identifying heterozygous deletions **(Fig. 3f)**. Using the same assay design, we confirmed that 5 of 5

159 randomly selected homozygous mutants carried 2 copies of the *Chd2* locus (**Fig. 3f**), validating
160 our conclusion that RAD51 enhances zygotic IHR.

161 Our data demonstrate that RAD51 enhances interhomolog repair and that this
162 enhancement can be leveraged for both donor-free homozygous conversion and *de novo*
163 homozygous KI. To our knowledge, our results are also the first to definitively show the
164 existence of IHR events in mammalian zygotes. Although previous work has suggested the
165 existence of these events, a recent commentary in *bioRxiv* highlights the need for more rigorous
166 analyses to confirm such findings and outlines 3 main points[18]. First, Egli *et al.* argue that
167 because IHR requires physical interaction of the maternal and paternal genomes, there must be a
168 sufficient explanation for how IHR can result from Cas9-mediated DSBs that occur while the
169 maternal and paternal genomes are segregated in separate pronuclei. Second, they suggest that
170 parthenogenesis must be ruled out as a possibility for the observed loss-of-heterozygosity. Last,
171 they suggest that additional measures be taken to rule out the possibility that the observed loss-
172 of-heterozygosity is due to large NHEJ-induced indels emanating from the Cas9 cut site. Our
173 data fulfills all three requirements and further goes on to show that RAD51 is capable of
174 significantly enhancing IHR. With respect to the need for physical proximity between homologs
175 to allow IHR, previous kinetic studies have shown that Cas9 can remain bound to its cut site for
176 up to 6 hours[19], which would be long enough to allow mitotic association of the maternal and
177 paternal alleles in mouse zygotes. Furthermore, an additional study in mouse demonstrated
178 successful correction of a disease mutation in zygotes without the use of exogenous donor
179 DNA[20], supporting the existence of a zygotic IHR mechanism. With regard to the ruling out
180 parthenogenesis, our experimental design relied upon transfer of the paternal mutation to the
181 maternal allele, excluding the possibility of a parthenogenesis-based mechanism. Last,

previously published work mouse zygotes showed that the median deletion size associated with a Cas9-induced cut with a single sgRNA was ~10bp, that deletions do not surpass 600bp, and that the occurrence of large deletions (>100bp) was largely sequence-dependent and far too infrequent to account for the high rates of IHR observed in our experiments[10]. In accordance with these findings, our copy-number analyses and F_1 genotyping data rule out large deletions as the source of loss-of-heterozygosity and therefore support our conclusions regarding the existence and enhancement of zygotic IHR.

Together, our studies validate the existence of a bona fide IHR-based DSB repair mechanism in the mammalian zygote and demonstrate significant enhancement of this process by the HDR-associated strand exchange factor RAD51. Furthermore, we show that enhancement of the IHR and/or HDR pathways with exogenous RAD51 can be used for highly efficient homozygous KI and donor-free homozygous conversion. Ongoing efforts to generate primate models of human diseases have been hindered by low efficiency, long generation times, and high costs associated with obtaining homozygotes. However, our method has the potential to generate F_0 homozygotes with high efficiency, significantly decreasing costs and study length. Taken as a whole, our findings have broad implications for applications in basic sciences, disease modeling, therapeutic gene editing, and biotechnology.

Methods

Data Availability: The raw data supporting the findings in this manuscript can be obtained from the corresponding author upon reasonable request.

Animal Care and Use: All mouse work was performed with the supervision of the Massachusetts Institute for Technology Division of Comparative Medicine (DCM) under protocol 0416-024-19, which was approved by the Committee for Animal Care (CAC). All procedures were in accordance with the guidelines set forth by the Guide for Care and Use of Laboratory Animals, National Research Council, 1996 (institutional animal assurance no. A-3125-01). All embryos injected for the experiments described in this manuscript were on a C57BL/6NTac background (Taconic; referred to as C57BL/6N in paper).

Preparation of Injection Mixtures: tracrRNA, crRNAs, and ssODNs were synthesized by Integrated DNA Technologies (see Supplementary Table 1 for sequences). All injection mixtures were prepared in a final volume of 50μL according using the same protocol. Using RNase-free water, reagents, and consumables, crRNA (final concentration 0.61μM), tracrRNA (final concentration 0.61μM), and ultrapure Tris-HCl, pH7.39 (final concentration 10mM, ThermoFisher) were mixed and incubated at 95°C for 5 minutes. The mixtures were cooled to room temperature for 10 minutes on the benchtop and then EnGen Cas9-NLS (New England Biolabs) was added to a final concentration of 30ng/μL. The mixtures were incubated at 37°C for 15 minutes before adding any remaining components: ssODN (final concentration 30ng/μL), RAD51 (Creative Biomart, final concentration 10ng/μL). Injection mixtures were stored on ice and briefly heated to 37°C prior to injection. For experiments utilizing RS-1, embryos were cultured in KSOM-AA with 7.5μM RS-1 (Sigma) or DMSO (Sigma, 1:1000) for 24 hours, washed, and cultured in standard FHM until collection for genotyping.

In Vitro Fertilization: *In vitro* fertilization was performed using FERTIUP® Mouse Preincubation Medium and CARD MEDIA (Kyudo Company) according to the manufacturer's protocol.

227 ***Zygotic Injections:*** Female mice (4-5 weeks old, C57BL/6NJ) were superovulated by IP
228 injection of PMS (5 IU/mouse, three days prior to microinjection) and hCG (5 IU/mouse, 47
229 hours after PMS injection), and paired with males. Plugged females were sacrificed by cervical
230 dislocation at day 0.5pcd and zygotes were collected into 0.1% hyaluronidase/FHM. Zygotes
231 were washed in drops of FHM and cumulus cells were removed. Zygotes were cultured in
232 KSOM-aa medium for one hour and used for microinjection. Pronuclear injection was performed
233 using a micromanipulator (Narishige), microscope (Nikon), and injector (Eppendorf). Zygotes
234 were cultured until collection for genotyping. For experiments giving rise to F_0 animals, embryos
235 were surgically implanted into pseudopregnant CD-1 females (Charles River Laboratories, Strain
236 Code 022) 24 hours post-injection, allowed to develop normally, and recovered following natural
237 birth.
238 ***Embryo DNA Purification***: Embryos were collected at morula stage in 6µL embryo digestion
239 buffer (125µg/mL proteinase K, 100mM Tris-HCl pH 8.0, 100mM KCl, 0.02% gelatin, 0.45%
240 Tween-20, 60µg/mL yeast tRNA) and digested for 1 hour at 56°C. Proteinase K was inactivated
241 via incubation at 95°C for 10 minutes. Embryo DNA was stored at -20°C until use.
242 ***Tail DNA Purification***: Tail snips (~0.5cm length) were collected from animals, placed in 75µL
243 alkaline lysis buffer (25mM NaOH, 0.2mM EDTA), and incubated at 95°C for 30 minutes.
244 Digestion was stopped via addition of 75µL neutralization buffer (40mM Tris-HCl pH 5.0).
245 Samples were stored at 4°C until genotyping.
246 ***Chd2^{R1684H} Genotyping*:** Initial PCR was performed using either 3µL embryo DNA or 2µL
247 purified tail DNA. The longer amplification of the nested PCR reaction was performed using the
248 Chd2-RH_Long_F/R primer pair listed in Supplementary Table 2 and an annealing temperature

of 65°C. Nested PCR was performed using 2µL of the initial 25µL PCR reaction, the Chd2-RH_F/R primer pair listed in Supplementary Table 2, and an annealing temperature of 65°C.

Tyr^{C89S} Genotyping: Initial PCR was performed using 2µL purified tail DNA. The longer amplification of the nested PCR reaction was performed using the Tyr_Long_F/R primer pair listed in Supplementary Table 2 and an annealing temperature of 65°C. Nested PCR was performed using 2µL of the initial 25µL PCR reaction, the Tyr_F/R primer pair listed in Supplementary Table 2, and an annealing temperature of 65°C.

Genomic qPCR: To determine copy number at specific genomic loci, we developed a strategy utilizing multiplex nested qPCR. We first performed multiplex amplification of both the edited *Chd2* region and a region of the *Gapdh* promoter, which is located on a different chromosome, in a short round of PCR (10 cycles). In the case of our *Shank3B* control experiment, we attempted to match the input DNA concentration used for experiments utilizing DNA from cultured embryos. Based on an estimation of ~6pg DNA per cell and a PCR input of ~30 cells, we used 180pg *Shank3B*$^{+/+}$ or *Shank3B*$^{+/-}$ genomic DNA per initial reaction. We then used the PCR products from the initial multiplex PCR as input for subsequent qPCR using Sso Advanced SYBR Green Supermix (Bio-Rad). qPCR was performed on a CFX96 Touch Real-Time PCR Detection System (Bio-Rad) and analyzed using CFX Maestro software (Bio-Rad). *Chd2* or *Shank3B* signal was normalized to *Gapdh* signal to control for input and a second diploid locus.

Statistical Analyses: Statistical analyses were performed using Prism 6 (Graphpad). For initial experiments in which the effects of RS-1 and RAD51 were unknown, as well as mixed oligo KI experiments where RAD51 could potentially increase either compound heterozygosity or homozygosity, two-tailed analyses were used. All other experiments exploring RAD51's ability

271 to increase KI and homozygous KI efficiencies utilized one-tailed tests. Genomic qPCR

272 performed in Figure 3 was analyzed by unpaired t-test. The graph displays mean±SEM.

273

274 **References**

275

276 1. Aida, T. *et al.* Cloning-free CRISPR/Cas system facilitates functional cassette knock-in in
277 mice. *Genome Biol* **16,** 87 (2015).
278 2. Quadros, R. M. *et al.* Easi-CRISPR: a robust method for one-step generation of mice
279 carrying conditional and insertion alleles using long ssDNA donors and CRISPR
280 ribonucleoproteins. *Genome Biol* **18,** 103 (2017).
281 3. Aida, T. *et al.* Gene cassette knock-in in mammalian cells and zygotes by enhanced
282 MMEJ. *BMC Genomics* **17,** 183 (2016).
283 4. Yu, C. *et al.* Small Molecules Enhance CRISPR Genome Editing in Pluripotent Stem
284 Cells. *Cell Stem Cell* **16,** 142–147 (2015).
285 5. Li, G. *et al.* Small molecules enhance CRISPR/Cas9-mediated homology-directed genome
286 editing in primary cells. *Sci. Rep.* **7,** 8943 (2017).
287 6. Song, J. *et al.* RS-1 enhances CRISPR/Cas9- and TALEN-mediated knock-in efficiency.
288 *Nature Communications* **7,** 10548 (2016).
289 7. Maruyama, T. *et al.* Increasing the efficiency of precise genome editing with CRISPR-
290 Cas9 by inhibition of nonhomologous end joining. *Nature Biotechnology* **33,** 538–542
291 (2015).
292 8. Ma, X. *et al.* CRISPR/Cas9-mediated gene manipulation to create single-amino-acid-
293 substituted and floxed mice with a cloning-free method. *Sci. Rep.* **7,** 42244 (2017).
294 9. Paquet, D. *et al.* Efficient introduction of specific homozygous and heterozygous
295 mutations using CRISPR/Cas9. *Nature* **533,** 125–129 (2016).
296 10. Shin, H. Y. *et al.* CRISPR/Cas9 targeting events cause complex deletions and insertions at
297 17 sites in the mouse genome. *Nature Communications* **8,** 15464 (2017).
298 11. Ghodsinejad Kalahroudi, V. *et al.* Two Novel Tyrosinase (TYR) Gene Mutations with
299 Pathogenic Impact on Oculocutaneous Albinism Type 1 (OCA1). *PLoS ONE* **9,** e106656
300 (2014).
301 12. Takayama, K. *et al.* Highly efficient biallelic genome editing of human ES/iPS cells using
302 a CRISPR/Cas9 or TALEN system. *Nucleic Acids Research* **45,** 5198–5207 (2017).
303 13. McVey, M. & Lee, S. E. MMEJ repair of double-strand breaks (director's cut): deleted
304 sequences and alternative endings. *Trends in Genetics* **24,** 529–538 (2008).
305 14. Richardson, C., Moynahan, M. E. & Jasin, M. Double-strand break repair by
306 interchromosomal recombination: suppression of chromosomal translocations. *Genes &*
307 *Development* **12,** 3831–3842 (1998).
308 15. Moynahan, M. E. & Jasin, M. Loss of heterozygosity induced by a chromosomal double-
309 strand break. *Proc Natl Acad Sci USA* **94,** 8988–8993 (1997).
310 16. Ma, H. *et al.* Correction of a pathogenic gene mutation in human embryos. *Nature* **548,**
311 413–419 (2017).
312 17. Peca, J. *et al.* Shank3 mutant mice display autistic-like behaviours and striatal
313 dysfunction. *Nature* **472,** 437–442 (2011).

18. Egli, D., Zuccaro, M., Kosicki, M., Church, G. & Bradley, A. Inter-homologue repair in fertilized human eggs? *bioRxiv* (2017). doi:10.1101/181255
19. Richardson, C. D., Ray, G. J., DeWitt, M. A., Curie, G. L. & Corn, J. E. Enhancing homology-directed genome editing by catalytically active and inactive CRISPR-Cas9 using asymmetric donor DNA. *Nature Biotechnology* **34,** 339–344 (2016).
20. Wu, Y. *et al.* Correction of a Genetic Disease in Mouse via Use of CRISPR-Cas9. *Cell Stem Cell* **13,** 659–662 (2013).

Acknowledgements

The experiments described in this manuscript were funded by the Tan-Yang Center for Autism Research at MIT and the Poitras Center for Affective Disorders Research at MIT. We would like to thank Tetsushi Sakuma and Takashi Yamamoto of Hiroshima University for sharing their knock-in enhancer screening data. Lastly, we are grateful for the helpful discussion and insight provided by members of the Feng lab.

Author Contributions

J.J.W., T.A., M.W., Q.Z., and G.F. designed experiments. J.J.W. and P.Q. performed experiments. J.J.W., T.A., M.W., and G.F. analyzed data. J.J.W., T.A., and G.F. prepared the manuscript.

Competing Financial Interests

The authors of this manuscript declare no competing financial interests.

Materials and Correspondence

Correspondence and materials requests should be addressed to G.F. at fengg@mit.edu

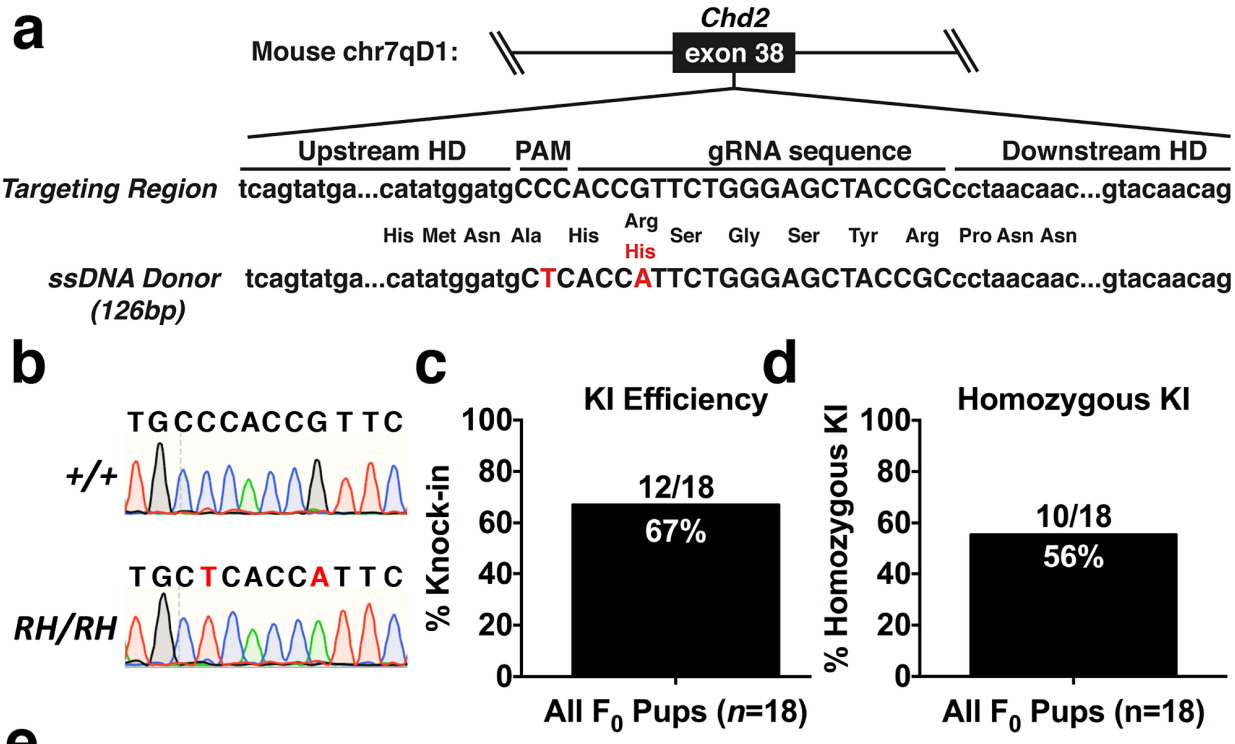

e

Father ID (Genotype)	Mother ID (Genotype)	F_1 Het Pups
C57BL/6N (+/+)	9989 (*RH/RH*)	8/8
C57BL/6N (+/+)	9991 (*RH/RH*)	4/4
C57BL/6N (+/+)	9995 (*RH/RH*)	6/6
9992 (*RH/RH*)	C57BL/6N (+/+)	6/6
9994 (*RH/RH*)	C57BL/6N (+/+)	9/9
10000 (*RH/RH*)	C57BL/6N (+/+)	3/3

Figure 1: Efficient homozygous knock-in with RAD51. a, Schematic of the targeting locus and HR donor for generating *Chd2*^{R1684H} mutant mice. HR donor contains both the c.5051G>A point mutation and a synonymous mutation that destroys the relevant PAM site (HD=homology domain). **b,** Example chromatograms of wildtype (top) and *Chd2*$^{R1684H/R1684H}$ animals (RH=R1684H). **c,** Overall KI efficiency observed in F_0 pups (pups with ≥1 KI allele/total pups). **d,** Homozygous KI rate observed in F_0 pups. **e,** Genotyping results from F_1 pups derived from crosses between F_0 *Chd2*$^{R1684H/R1684H}$ animals and wildtype C57BL/6N animals.

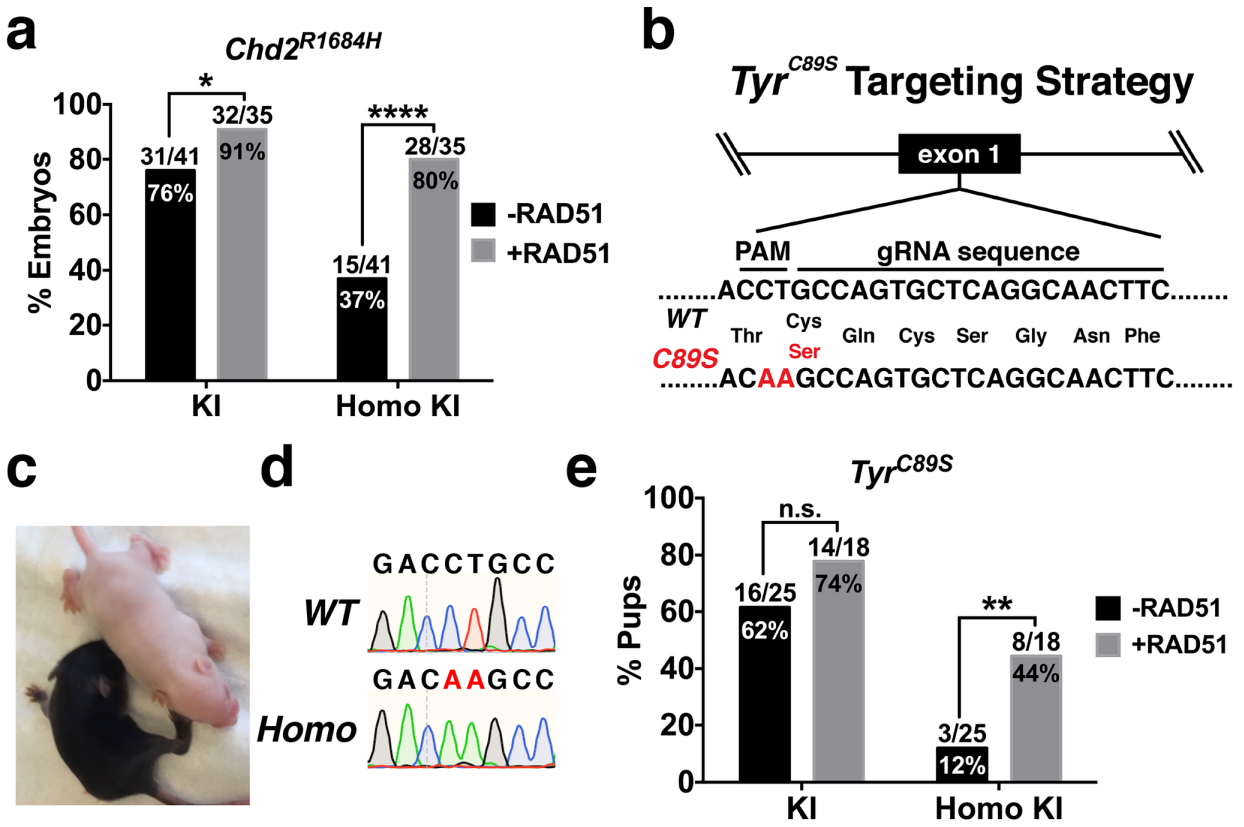

Figure 2: Exogenous RAD51 enhances KI efficiency at multiple loci. a, *Chd2*^{R1684H} PNI using 30ng/μL ssODN with or without RAD51 revealed a slight increase in overall KI efficiency ($p<0.05$, one-tailed chi-square test) and a dramatic increase in homozygous KI efficiency ($p<0.0001$, one-tailed chi-square test). **b,** Schematic of knock-in strategy for the albinism-associated *Tyr*^{C89S} mutation. **c,** Representative examples of *Tyr*$^{+/+}$ (black) and *Tyr*$^{C89S/C89S}$ (white) littermates derived from three-component CRISPR injections using exogenous RAD51. **d,** Representative chromatograms from *Tyr*$^{+/+}$ (top) and *Tyr*$^{C89S/C89S}$ animals. **e,** Genotyping of F_0 animals generated by three-component CRISPR with or without RAD51 showed no significant effect of RAD51 on overall KI efficiency (n.s.=not significant, $p=0.166$, one-tailed chi-square test), but a significant RAD51-dependent increase in homozygous KI rates ($p=0.0081$, one-tailed chi-square test).

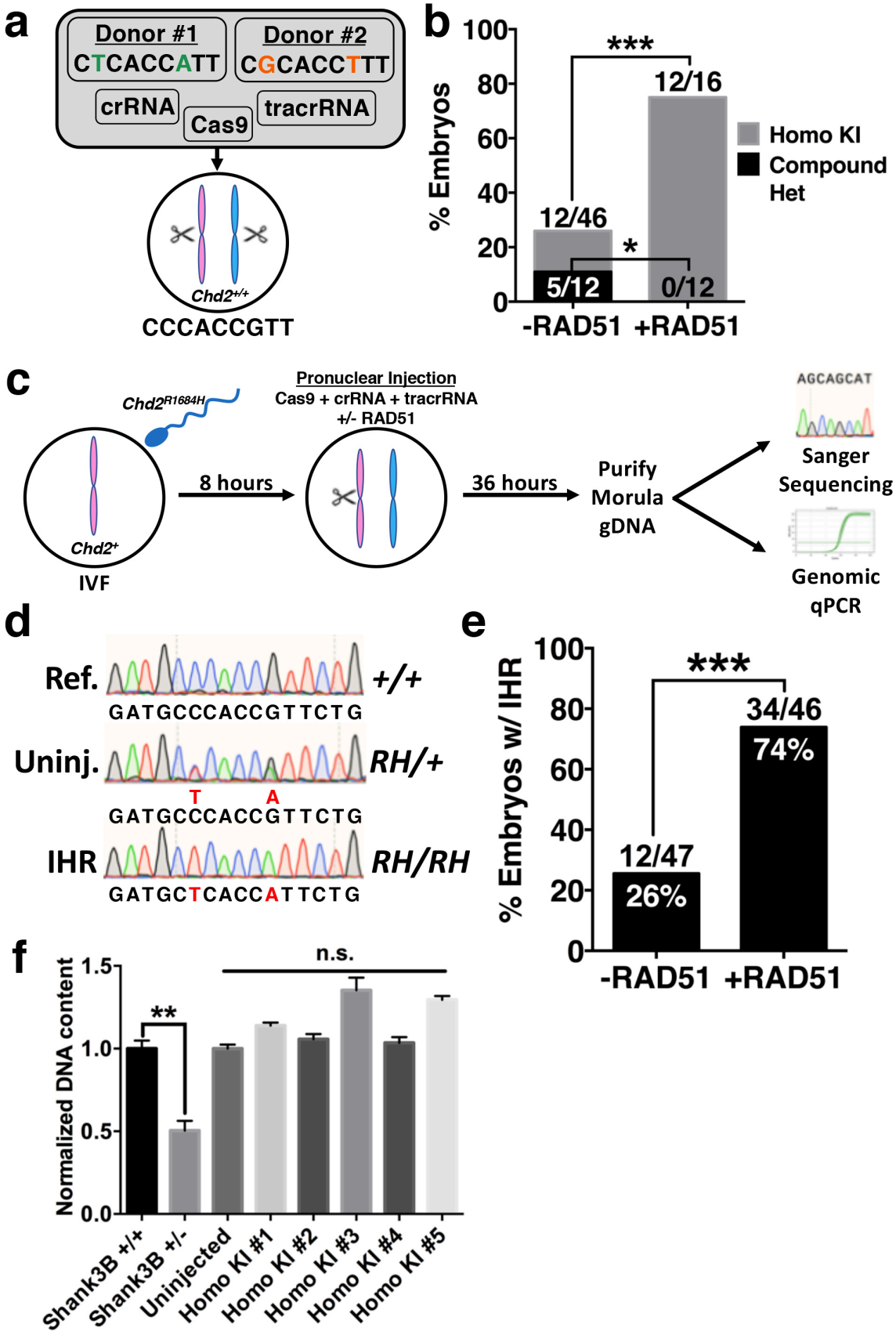

Figure 3: RAD51 enhances interhomolog repair. a, Schematic of strategy to test homozygous KI mechanism. Fertilized embryos were injected with Cas9 protein, crRNA, tracrRNA, and an equimolar mixture of two ssODNs varying by two nucleotides with or without RAD51 protein. **b,** Genotyping results from embryos collected following mixed ssODN injection. Homozygous KI efficiency represents the fraction of homozygous KI events observed in all injected embryos ($p=0.0008$, one-tailed chi-square test). Compound heterozygous rates represent the fraction of homozygous KI embryos with a different KI event on each allele ($p=0.0120$, two-tailed chi-square test). **c,** Schematic of strategy for testing RAD51-enhanced IHR. Wildtype C57BL/6N eggs were fertilized *in vitro* by sperm collected from male *Chd2*$^{R1684H/R1684H}$ mice and cultured for 8 hours. At 8hpf, PNI was performed with Cas9 protein, crRNA, and tracrRNA with or without RAD51 protein. Since *R1684H* mutants carry a mutation in the PAM associated with the crRNA utilized in these experiments, Cas9 is only capable of cutting the maternal allele. Injected embryos were then cultured for 48 hours and collected at morula stage. Half of the purified DNA was used for nested PCR and Sanger sequencing and the other half was used for multiplex PCR and subsequent qPCR to analyze genomic copy number at the *Chd2* editing locus. **d,** Representative chromatograms showing the wildtype reference sequence (Ref., top), an uninjected *Chd2*$^{R1684H/+}$ embryo generated by IVF (Uninj., middle), and a *Chd2*$^{R1684H/R1684H}$ homozygous mutant (IHR, bottom) generated via donor-free, RAD51-enhanced three-component CRISPR. **e,** Sanger sequencing of IVF-derived embryos revealed a significant increase in IHR in embryos injected with RAD51 ($p<0.0001$, one-tailed chi-square test). **f,** Genomic qPCR targeting *Shank3B* using 180pg genomic DNA from wildtype and *Shank3B*$^{+/-}$ mice indicate that our copy-number strategy is capable of identifying heterozygous deletions (lanes 1-2, $p=0.00295$, unpaired t-test, $t=6.47$, $df=4$, $n=3$ technical replicates per sample, error bars=SEM). qPCR using DNA from an uninjected embryo and 5 randomly selected homozygous *Chd2*^{R1684H} embryos revealed normal copy number at the *Chd2* editing locus in all animals (lanes 3-8, $p>0.05$, unpaired t-test, $t=4.60$, $df=6$, $n=4$ technical replicates per sample, error bars=SEM)**.**

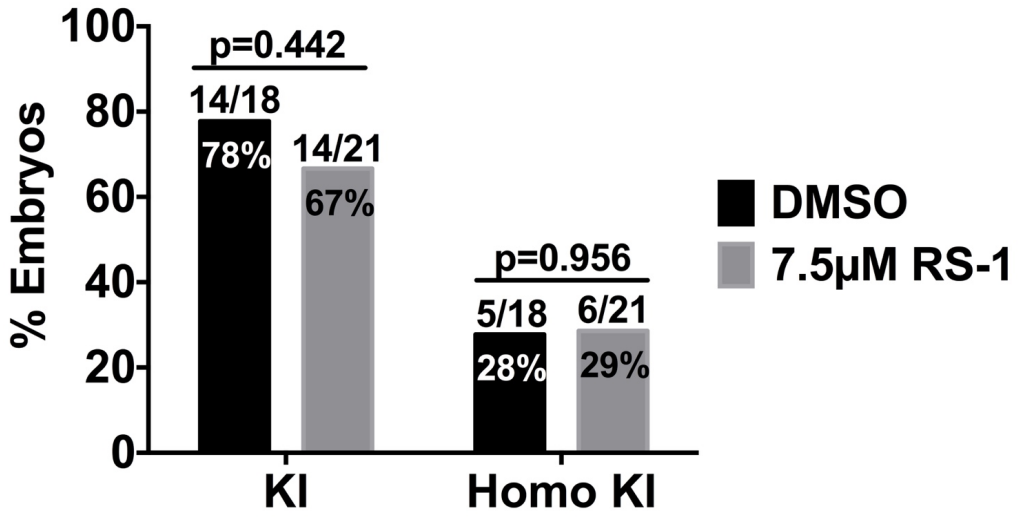

Extended Data Figure 1: RS-1 does not alter KI efficiency in mouse zygotes. Genotyping of morula-stage embryos cultured for 24 hours in either DMSO (1:1000 final concentration) or 7.5µM RS-1 showed no significant difference in overall KI efficiency or homozygous KI efficiency (two-tailed chi-square test).

a

Sex	Injection Type	Genotype	Notes
Female	CPI	RH/RH	
Female	CPI	RH/Indel	
Female	CPI	RH/RH	
Male	CPI	RH/RH	
Male	CPI	RH/RH	
Female	CPI	Indel/Indel	Same Indel
Female	CPI	RH/Indel	
Female	CPI	RH/RH	
Male	CPI	Indel/Indel	Different Indels
Female	PNI	RH/RH	
Male	PNI	RH/RH	
Male	PNI	RH/RH	
Female	PNI	Indel/Indel	Different Indels
Male	PNI	Indel/Indel	Same Indel
Male	PNI	RH/RH	
Male	PNI	Indel/Indel	Same Indel
Female	PNI	Indel/Indel	Same Indel
Female	PNI	RH/RH	

b

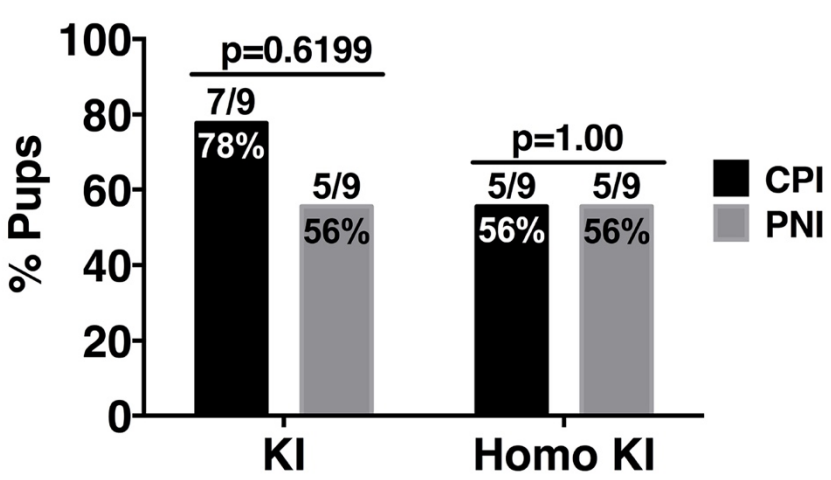

Extended Data Figure 2: Confirmation of F_0 homozygosity. **a,** Genotyping results for all F_0 pups obtained from either cytoplasmic (CPI) or pronuclear (PNI) injections for *Chd2*^{R1684H} knock-in experiments described in Figure 1. **b,** Quantification of overall KI efficiency (left) and homozygous KI efficiency (right) shows no significant difference in KI rates when comparing CPI and PNI strategies (two-tailed chi-square test).

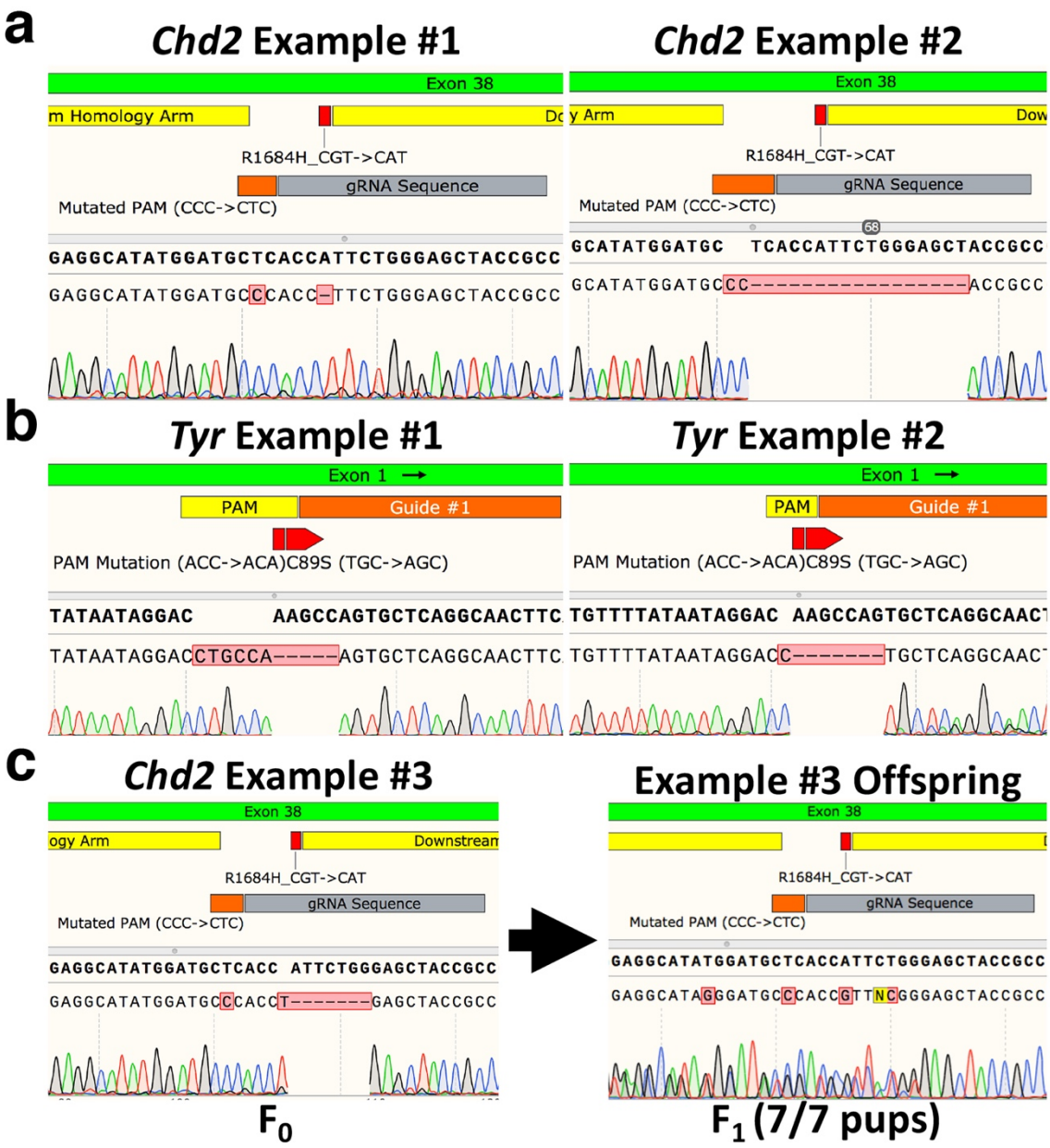

Extended Data Figure 3: RAD51 stimulates the generation of homozygous indels. a, Representative Sanger sequencing traces of putative homozygous indels observed in F_0 animals obtained from *Chd2*^{R1684H} knock-in experiments. **b,** Representative Sanger sequencing traces of putative homozygous indels observed in F_0 animals obtained from *Tyr*^{C89S} knock-in experiments. **c,** Genotyping traces for a putative homozygous *Chd2* indel and an F_1 offspring from a cross between the founder and a wildtype C57BL/6N mate. The F_1 genotyping, which was consistent for all 7 pups in the litter, indicates heterozygous presence of the indel observed in the founder.

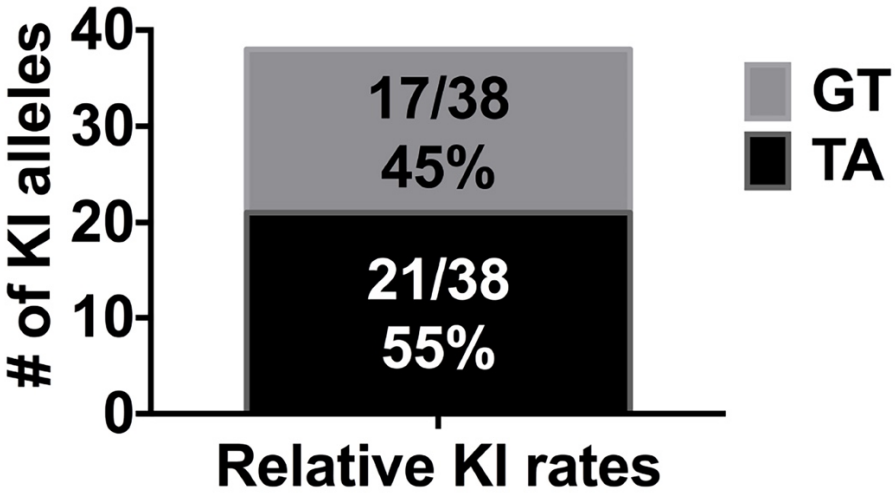

Extended Data Figure 4: TA (*Chd2*^{R1684H}) and GT donors show unbiased knock-in efficiencies. Quantification of KI rates observed for the TA (standard *Chd2*^{R1684H} donor) and GT donors used in Figure 2d shows no significant difference (two-tailed chi-square test).

Component	Sequence
tracrRNA	AAACAGCAUAGCAAGUUAAAAUAAGGCUAGUCCGU UAUCAACUUGAAAAAGUGGCACCGAGUCGGUGCU
Chd2^{R1684H} crRNA	GCGGUAGCUCCCAGAACGGUGUUUUAGAGCUAUGC UGUUUUG
Chd2^{R1684H} ssODN	TCAGTATGAGCAGCATTGGTATAAGGACCACCACTA TGGTGACCGGAGGCATATGGATGCTCACCATTCTGG GAGCTACCGCCCTAACAACATGTCCAGAAAGAGGCC GTATGAGCAGTACAACAG
Chd2^{GT} Variant Donor	TCAGTATGAGCAGCATTGGTATAAGGACCACCACTA TGGTGACCGGAGGCATATGGATGC CACCTTTCTGG GAGCTACCGCCCTAACAACATGTCCAGAAAGAGGCC GTATGAGCAGTACAACAG
Tyr^{C89S} crRNA	GAAGUUGCCUGAGCACUGGCGUUUUAGAGCUAUGC UGUUUUG
Tyr^{C89S} ssODN	GTTCCCCTTCAAAGGGGTGGATGACCGTGAGTCCTGG CCCTCTGTGTTTTATAATAGGACAAGCCAGTGCTCAG GCAACTTCATGGGTTTCAACTGCGGAAACTGTAAGTT TGGATTTGGGG

Supplementary Table 1: Sequences of Injection Components. Guide sequences are highlighted in red.

505

Forward Primer	Sequence	Reverse Primer	Sequence	Product Size (bp)
Chd2-RH_Long_F	ACTGACACATGGGAGAAGCC	Chd2-RH_Long_R	TCTCCTTATAACAGGCCAACC	429
Chd2-RH_F	AGTGCCTCACCTCTCACACC	Chd2-RH_R	ACTGGCAGAGGGAAAGAAAG	266
Tyr_Long_F	TCAATTTAGTTACCTCACTATGGGC	Tyr_Long_R	CAAGTACTCATCTGTGCAAATGTC	992
Tyr_F	TTTGGCCATAGGTGCCTG	Tyr _R	GAGCCTGTGCCTCCTCTAAG	411
Shank3_Long_F	AGGAAAGCAAGGTTGAGCTG	Shank3_Long_R	CTCTGAGGCTTGCAGACGG	584
Shank3_F	GAGCTCTACTCCCTTAGGACTT	Shank3_R	TCCCCCTTTCACTGGACACCC	316
Gapdh_Long_F	TACGGGTGCACGTAGCTCAG	Gapdh_Long_R	CGAAGGACACCAGGCAGTC	396
Gapdh_F	TCCCTAGACCCGTACAGTGC	Gapdh _R	CTCTGCTCCTCCCTGTTCC	133

506

507 **Supplementary Table 2: Sequences of PCR primers and expected product sizes.**

508
509
510
511
512
513
514
515
516
517
518
519
520
521
522
523
524
525
526
527
528
529
530